5072 *Chem. Mater.* **2009,** *21,* 5072–5078
DOI:10.1021/cm901536z

CHEMISTRY OF MATERIALS
Article

Defect Interactions in $Sr_3La(Fe,Al)_3O_{10-\delta}$ by Computer Simulations and Mössbauer Spectroscopy

Ekaterina V. Tsipis,[†] Eugene N. Naumovich,[‡] Mikhail V. Patrakeev,[§] Polyna V. Anikina,[§] João C. Waerenborgh,[†] and Vladislav V. Kharton*[,‡]

[†]*Chemistry Department, Instituto Tecnológico e Nuclear, CFMC-UL, EN 10, 2686-953 Sacavém, Portugal,* [‡]*Department of Ceramics and Glass Engineering, CICECO, University of Aveiro, 3810-193 Aveiro, Portugal, and* [§]*Institute of Solid State Chemistry, Ural Division of RAS, 91 Pervomayskaya Str., 620219 Ekaterinburg, Russia*

Received June 5, 2009. Revised Manuscript Received September 19, 2009

Moderate Al^{3+} doping in Ruddlesden−Popper type $Sr_3LaFe_3O_{10-\delta}$ leads to complete reconfiguration of the electronic sublattice. While oxygen vacancies, Fe^{4+}, and substitutional cations all exhibit energetic affinity for the equatorial perovskite-like planes, the atomistic computer simulations showed that Coulombic repulsion between the point defects and local lattice deformations near Al^{3+} result in hole displacement out of these layers when the content of vacant anion sites and/or aluminum is significant. The Al^{3+} cations tend to form relatively stable aluminum−oxygen tetrahedra, which are energetically favorable for the central perovskite layers and distort neighboring polyhedra formed by iron. These effects and partial hole localization in the apical iron−oxygen polyhedra adjacent to Al^{3+} were confirmed by Mössbauer spectroscopy analysis of $Sr_3LaFe_{3-x}Al_xO_{10-\delta}$ ($x = 0.3-0.6$, $\delta = 0-1$).

1. Introduction

Ferrite phases of the Ruddlesden−Popper (RP) family, with general formula $A_{n+1}B_nO_{3n+1}$ where A is the rare-earth and/or alkaline-earth element and B corresponds to iron and substitutional cations, attract great interest due to their unusual electrical, magnetic, and physicochemical properties.[1−7] In particular, fast oxygen-ionic transport in combination with predominant electronic conductivity and relatively good stability, important for potential applications in the dense ceramic membranes for oxygen separation and natural gas conversion, are known for the oxide materials derived from $Sr_3LaFe_3O_{10-\delta}$ where $n = 3$. Contrary to the perovskite-type analogues, layered ferrites exhibit a moderate thermal and chemical-induced expansion advantageous for the high-temperature electrochemical applications, although an essentially two-dimensional character of the transport processes in the oxygen-deficient RP phases leads usually to lower ionic and electronic conductivities.[4,6,8−10] The incorporation of cations with constant oxidation state, such as Al^{3+} or Sc^{3+}, makes it possible to further improve the dimensional stability and, often, ionic conduction.[7,11,12] For Al-substituted perovskites, these effects correlate with oxygen-vacancy trapping near Al^{3+} having a strong energetic affinity to tetrahedral coordination.[11,12]

The intergrowth crystal structure of $Sr_3LaFe_3O_{10}$-based compounds (Figure 1a) is built of triple perovskite-like $(Sr,La)FeO_{3-\delta}$ layers, which may accommodate significant oxygen deficiency (δ), and alternating rock-salt (Sr,La)O sheets. The neutron powder diffraction studies[2] showed that Al^{3+} incorporation occurs preferably in the equatorial B1 positions, while oxygen vacancies are formed in the O2 and O4 sites constituting the central perovskite blocks in the $Sr_3LaFe_3O_{10-\delta}$ lattice. Increasing oxygen deficiency in the RP ferrites is charge-compensated by lowering the concentration of p-type electronic charge carriers dominating under oxidizing conditions[4−8] and may result in progressive vacancy ordering up to the formation of brownmillerite-type slabs

*Corresponding author. Tel: +351-234-370263. Fax: +351-234-425300. E-mail: kharton@ua.pt.

(1) Barrier, N.; Pelloquin, D.; Nguyen, N.; Giot, M.; Bouree, F.; Raveau, B. *Chem. Mater.* **2005**, *17*, 6619.
(2) Lee, J. Y.; Swinnea, J. S.; Steinfink, H.; Reiff, W. M.; Pei, S.; Jorgensen, J. D. *J. Solid State Chem.* **1993**, *103*, 1.
(3) Kuzushita, K.; Morimoto, S.; Nasu, S.; Kawasaki, S.; Takano, M. *Solid State Commun.* **2002**, *123*, 107.
(4) Abbate, M.; Mogni, L.; Prado, F.; Caneiro, A. *Phys. Rev. B* **2005**, *71*, 195113.
(5) Manthiram, A.; Prado, F.; Armstrong, T. *Solid State Ionics* **2002**, *152−153*, 647.
(6) Patrakeev, M. V.; Leonidov, I. A.; Kozhevnikov, V. L.; Kharton, V. V. *Solid State Sci.* **2004**, *6*, 907.
(7) Markov, A. A.; Patrakeev, M. V.; Kharton, V. V.; Pivak, Y. V.; Leonidov, I. A.; Kozhevnikov, V. L. *Chem. Mater.* **2007**, *19*, 3980.
(8) Tsipis, E. V.; Kharton, V. V. *J. Solid State Electrochem.* **2008**, *12*, 1367.
(9) Al Daroukh, M.; Vashook, V. V.; Ullmann, H.; Tietz, F.; Arual Raj, I. *Solid State Ionics* **2003**, *158*, 141.
(10) Mogni, L.; Fouletier, J.; Prado, F.; Caneiro, A. *J. Solid State Chem.* **2005**, *178*, 2715.
(11) Patrakeev, M. V.; Kharton, V. V.; Bakhteeva, Yu.A.; Shaula, A. L.; Leonidov, I. A.; Kozhevnikov, V. L.; Naumovich, E. N.; Yaremchenko, A. A.; Marques, F. M. B. *Solid State Sci.* **2006**, *8*, 476.
(12) Naumovich, E. N.; Patrakeev, M. V.; Kharton, V. V.; Islam, M. S.; Yaremchenko, A. A.; Frade, J. R.; Marques, F. M. B. *Solid State Ionics* **2006**, *177*, 457.

 Published on Web 10/09/2009

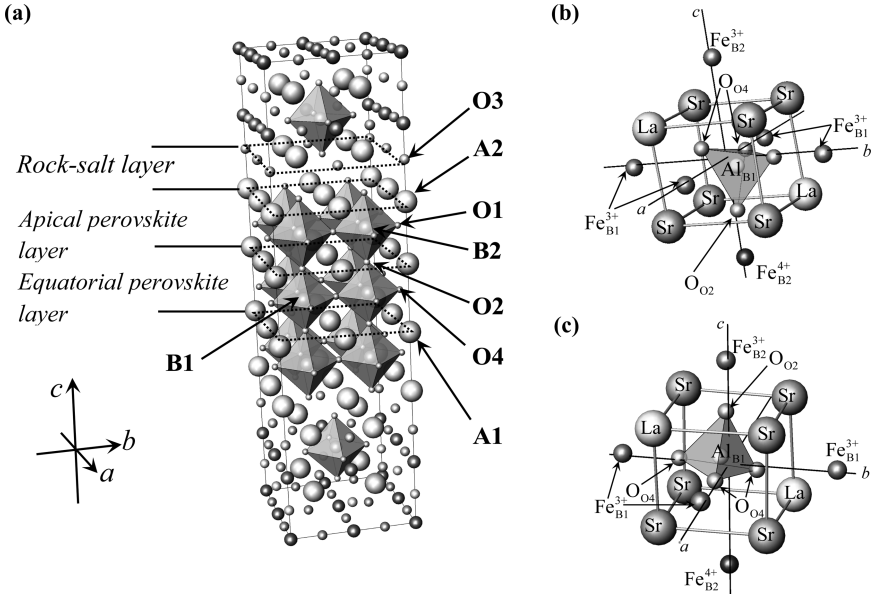

Figure 1. Crystal structure of $Sr_3La(Fe,Al)_3O_{10-\delta}$ (a) and calculated ion positions near one $Al^{3+}O_4$ tetrahedron forming moderately (b) and highly (c) unfavorable configurations with Fe^{4+} (see text and Table 2).

as demonstrated for $Sr_3NdFe_3O_9$.[1] As a result of Coulombic repulsion between the point defects and resultant site-exclusion effects known for the perovskites,[7,11,12] these processes can be expected to strongly influence the electronic sublattice, metal−oxygen bonding strength, and mixed ionic−electronic conductivity. However, information on the point-defect interaction mechanisms and state of the p-type electronic charge carriers in the RP ferrites is still scarce.

The present work is focused on the analysis of energetically favorable defect configurations and states of iron cations in RP-type $Sr_3La(Fe,Al)_3O_{10-\delta}$ by employing the static lattice computer simulations and ^{57}Fe transmission Mössbauer spectroscopy (MS). The techniques of atomistic modeling are often used to probe defect formation and reactions in oxide materials; the theoretical background, implications, and limitations of this method are well documented in the literature.[7,11−15] Well-known is also the capability of MS analysis to determine electronic states and local environment of iron cations in perovskite-related compounds. Particularly for the Fe^{4+}-containing RP and perovskite phases, valuable information may be obtained from the Mössbauer effect on the localization degree of σ^* (Fe 3d−O 2p) electrons which may either remain itinerant or give rise to charge disproportionation, $2Fe^{4+} \Leftrightarrow Fe^{5+} + Fe^{3+}$, on cooling below the Néel temperature T_N.[16−19] The latter situation was reported for oxidized $Sr_3LaFe_3O_{10}$ where the low-temperature Mössbauer spectra display only coexisting Fe^{3+} and Fe^{5+} states.[3]

2. Experimental Section

Single-phase $Sr_3LaFe_{3-x}Al_xO_{10-\delta}$ ($x = 0.3-0.6$, $\delta = 0-1$) were synthesized by the glycine-nitrate process,[20] with subsequent annealing in atmospheric air at 1170 and 1370 K for 25 h. Final sintering of dense ceramic disks compacted uniaxially at 200 MPa was performed at 1620 K in air during 10 h. The cation composition was confirmed by the inductively coupled plasma (ICP) spectroscopy using a Jobin Yvon instrument, model JY 70 plus. The powdered samples used for X-ray diffraction (XRD), thermogravimetric analysis (TGA), and Mössbauer spectroscopy studies were obtained by grinding of dense ceramics either after sintering or following an additional thermal treatment in the conditions specified below. For all materials studied in this work, XRD analysis (Rigaku D/Max-B instrument, Cu Kα radiation, $2\theta = 10-100°$, step 0.02°, 5 s/step) showed the formation of single tetragonal RP phases, space group $I4/mmm$, in agreement with structural data.[2] The oxygen content was calculated from the TGA results collected on complete reduction of $Sr_3La(Fe,Al)_3O_{10-\delta}$ into metallic iron and oxides of other components. The procedure of TGA (Setaram SetSys 16/18 instrument) included heating up to 1273 K in a dry air flow, temperature cycling in the range 973−1273 K with 50 K steps, and equilibration at each temperature during 3 h, as illustrated by the inset in Figure 2a. Following flushing of the apparatus with argon at 1373 K, the samples were reduced in a flowing dried 10% H_2−90% N_2 mixture for 50 h and then heated up to 1423 K in the same flow to ensure complete reduction of iron. One example of the isothermal reduction plot is presented in Figure 2a. Figure 2b shows the equilibrium δ values, which were collected in the regime of isothermal dwells and used to prepare compositions with different oxygen content. Slow cooling of $Sr_3LaFe_{2.7}Al_{0.3}O_{10-\delta}$ in air made it possible to obtain an almost negligible vacancy concentration; the measured oxygen deficiency in slowly cooled $Sr_3LaFe_{2.7}Al_{0.3}O_{10}$ was comparable to the experimental error ($\delta \approx 0.01$). The

(13) Gale, J. D.; Rohl, A. L. *Mol. Simul.* **2003**, *29*, 291.
(14) Freeman, G. M.; Catlow, V. R. A. *J. Solid State Chem.* **1995**, *85*, 65.
(15) Islam, M. S. *J. Mater. Chem.* **2000**, *10*, 1027.
(16) Battle, P. D.; Gibb, T. C.; Nixon, S. *J. Solid State Chem.* **1988**, *77*, 124.
(17) Dann, S. E.; Weller, M. T.; Currie, D. B.; Thomas, M. F.; Al-Rawwas, A. D. *J. Mater. Chem.* **1993**, *3*, 1231.
(18) Adler, P. *J. Mater. Chem.* **1999**, *9*, 471.
(19) Adler, P.; Ghosh, S. *Solid State Sci.* **2003**, *5*, 445.
(20) Kharton, V. V.; Waerenborgh, J. C.; Viskup, A. P.; Yakovlev, S.; Patrakeev, M. V.; Gaczyński, P.; Marozau, I. P.; Yaremchenko, A. A.; Shaula, A. L.; Samakhval, V. V. *J. Solid State Chem.* **2006**, *179*, 1273.

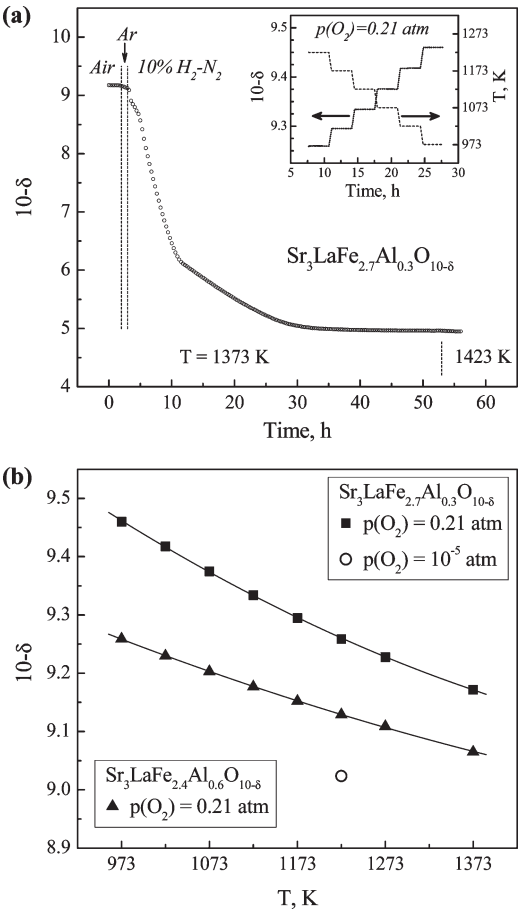

Figure 2. Determination of the total oxygen content in $Sr_3LaFe_{2.7}Al_{0.3}O_{10-\delta}$ on complete reduction in the H_2-containing atmosphere (a) and equilibrium oxygen deficiency of $Sr_3La(Fe,Al)O_{10-\delta}$ measured by TGA (b). Inset illustrates the equilibration procedure during isothermal steps in air.

composition where the predominant oxidation state of iron cations is 3+ ($\delta = 0.98$) was prepared by quenching after treatment in flowing argon at 1223 K (Figure 2b) during 25 h. In the case of $Sr_3LaFe_{2.4}Al_{0.6}O_{10-\delta}$, as-sintered material with an intermediate value of oxygen nonstoichiometry ($\delta = 0.28$) was used for the MS studies. Attempts to prepare reduced $Sr_3LaFe_{3-x}Al_xO_{10-\delta}$ ($x = 0.3-0.6$) via annealing in $H_2-H_2O-N_2$ atmospheres failed due to fast phase decomposition caused by the interaction with atmospheric water vapor and CO_2 at room temperature; partial decomposition was also observed for $Sr_3LaFe_{2.4}Al_{0.6}O_{10-\delta}$ annealed in flowing argon.

The Mössbauer spectra of the absorbers containing 5 mg/cm^2 of natural Fe were collected at 4.2 and 295 K using a constant-acceleration spectrometer equipped with a 25 mCi ^{57}Co (Rh) source and a JANIS SVT-400 bath cryostat. The velocity scale was calibrated using α-Fe foil. The equipment, experimental details, and fitting procedures were described in previous works (see refs 20 and 21 and references cited). The room-temperature spectra were fitted to Lorentzian lines using a nonlinear least-squares method; the relative areas and widths of both peaks in a quadrupole doublet were kept equal during refinement. The magnetically split spectra were fitted to distributions of magnetic sextets according to the histogram method.[22]

Table 1. Relative Energetic Effects for Various Point-Defect Locations in the Sr_3LaFeO_{10} Structure

defects and location	reference state	ΔE (eV)
V_{O1}	V_{O4}	0.52
V_{O2}		0.03
V_{O3}		0.75
$Fe^{4+}_{B1o} + Fe^{3+}_{B2o}$	$Fe^{4+}_{B2o} + Fe^{3+}_{B1o}$	−0.44
$Al^{3+}_{B1o} + Fe^{3+}_{B2o}$	$Al^{3+}_{B2o} + Fe^{3+}_{B1o}$	0.10
$Al^{3+}_{B1p} + Fe^{3+}_{B2p}$	$Al^{3+}_{B2p} + Fe^{3+}_{B1p}$	−0.46
$Al^{3+}_{B1t} + Fe^{3+}_{B2o}$	$Al^{3+}_{B2t} + Fe^{3+}_{B1o}$	−1.10
$Fe^{2+}_{B1o} + Fe^{3+}_{B2o}$	$Fe^{2+}_{B2o} + Fe^{3+}_{B1o}$	0.53
$Fe^{2+}_{B1p} + Fe^{3+}_{B2p}$	$Fe^{2+}_{B2p} + Fe^{3+}_{B1p}$	0.70
$Fe^{2+}_{B1t} + Fe^{3+}_{B2o}$	$Fe^{2+}_{B2t} + Fe^{3+}_{B1o}$	−0.17

The static-lattice computer simulation studies based on the Born model for ionic solids were performed using the GULP software;[13] the modeling procedures were similar to those used earlier for $(Sr,La)(Fe,M)O_{3-\delta}$ (M = Al, Ga) perovskites and RP-type $Sr_3(Fe,Sc)O_{7-\delta}$.[7,11,12] For this method, the ion charges determining long-range Coulombic forces are considered equal to the formal oxidation states, while the short-range interactions are described by the Pauli repulsion and Van der Waals dispersion models, expressed by the standard Bukingham potential. The interatomic potential parameters and the properties of ions were taken from the literature.[11,12,14] The simulations of various point-defect configurations, based on the Mott-Littleton approach, were carried out using a supercell consisting of 850 sites and having two overall compositions, namely, oxygen-deficient $Sr_3LaFe_3O_{9.44}$ and essentially stoichiometric $Sr_3LaFe_3O_{10}$ with one or two introduced vacancies. At the second stage of simulations, one iron cation occupying the B1 or B2 site was substituted with Al^{3+}; the location of all other ions in the corresponding crystallographic positions was fixed similar to the Al-free supercells, thus preserving local point-defect configurations. More than 200 configurations of Fe^{3+}, Fe^{4+}, Fe^{2+}, Al^{3+}, La^{3+}, and Sr^{2+} cations, O^{2-} anions, and oxygen vacancies (V_O), nearest-neighboring the B1 and B2 sites under consideration, were tested. In the discussion below, the crystallographic position of each ion or defect is denoted by the first subscript index used in the Kröger-Vink notation; the symbols $\overline{B}$ and $\overline{O}$ are used when the energetic effects are averaged for all relevant B or O sites, respectively. The additional subscript indices "t", "pl", "p", and "o" denote tetrahedral, fourfold planar, pyramidal, and octahedral oxygen coordination of the *B*-site cations, correspondingly.

3. Results and Discussion

The computer simulation studies confirmed that oxygen vacancy formation in $Sr_3La(Fe,Al)_3O_{10-\delta}$ occurs preferably in the O4 and O2 positions located in the central perovskite layer, in agreement with the neutron diffraction data.[2] The generation of interstitial oxygen anions via Frenkel disordering mechanism was found unlikely. Table 1 summarizes the calculated energy increments corresponding to the placement of one vacancy in the O1, O2, and O3 sites with respect to O4. While V_{O4} and V_{O2} are almost equivalent from the energetic point of

(21) Kharton, V. V.; Patrakeev, M. V.; Waerenborgh, J. C.; Kovalevsky, A. V.; Pivak, Y. V.; Gaczyński, P.; Markov, A. A.; Yaremchenko, A. A. *J. Phys. Chem. Solids* **2007**, *68*, 355.

(22) Hesse, J.; Rübartsch, A. *J. Phys. E* **1974**, *7*, 526.

Table 2. Relative Energetic Effects for the Formation of Various Defect Configurations in $Sr_3LaFeO_{10-\delta}$

δ	configuration	reference state	nearest neighborhood	ΔE (eV) min.	ΔE (eV) max.	ΔE (eV) average	N_{conf}[a]
0.56	$Al^{3+}_{B1p}-V_{\overline{O}}$	$Fe^{3+}_{B1p}-V_{\overline{O}}$	V_O, 2 La^{3+} and 6 Sr^{2+}	−0.75	−0.27	−0.50	6
	$Fe^{2+}_{B1p}-V_{\overline{O}}$			−1.23	−1.00	−1.10	6
	$Fe^{4+}_{B1p}-V_{\overline{O}}$			1.08	1.31	1.16	6
	$Fe^{2+}_{B1p} + Fe^{4+}_{Bo}$	$Fe^{3+}_{Blp} + Fe^{3+}_{Bo}$	V_O, 2 La^{3+} and 6 Sr^{2+}	−0.06	0.18	0.09	6
	$V_{\overline{O}}-Fe^{3+}_{B1t}-V_{\overline{O}}$	sum of all considered defects in the isolated state	2 V_O, 2 La^{3+} and 6 Sr^{2+}	0.55	1.65	1.03	13
	$V_{\overline{O}}-Fe^{3+}_{B1pl}-V_{\overline{O}}$			2.42	2.53	2.48	2
	$V_{\overline{O}}-Al^{3+}_{B1t}-V_{\overline{O}}$			−1.29	0.12	−0.54	15
	$V_{\overline{O}}-Fe^{2+}_{B1t}-V_{\overline{O}}$			−2.07	−0.77	−1.43	12
	$V_{\overline{O}}-Fe^{2+}_{B1pl}-V_{\overline{O}}$			−0.87	−0.54	−0.73	3
	$V_{\overline{O}}-Fe^{3+}_{B1t}-V_{\overline{O}}$		2 V_O, 3 La^{3+} and 5 Sr^{2+}	0.78	1.80	1.12	14
	$V_{\overline{O}}-Fe^{3+}_{B1pl}-V_{\overline{O}}$					2.43	1
	$Fe^{4+}_{B0}-O^{2-}_{\overline{O}}-Fe^{2+}_{Blt}$	$Fe^{3+}_{B0}-O^{2-}_{\overline{O}}-Fe^{3+}_{Blt}$	2 V_O, 2 La^{3+} and 6 Sr^{2+}	−2.59	−0.95	−1.72	17
	$Fe^{4+}_{Bp}-V_{\overline{O}}-Fe^{2+}_{Blt}$	$Fe^{3+}_{Bp}-V_{\overline{O}}-Fe^{3+}_{Blt}$		−0.93	−0.39	−0.68	12
~0	$Fe^{4+}_{B1o}-O^{2-}_{\overline{O}}-Al^{3+}_{B1t}$	$Fe^{4+}_{Bo}-O^{2-}_{\overline{O}}-Al^{3+}_{Blo}$, isolated Al^{3+}_{B1t}		0.70	1.32	0.99	24
	$Fe^{4+}_{B2o}-O^{2-}_{\overline{O}}-Al^{3+}_{B1t}$			0.65	1.54	0.88	10
	$Fe^{4+}_{Bp}-V_{\overline{O}}-Al^{3+}_{B1t}$			1.4	1.7	1.60	12
	$Fe^{4+}_{Bo}-O^{2-}_{\overline{O}}-Al^{3+}_{Blo}$	$Fe^{4+}_{Bo}-O^{2-}_{\overline{O}}-Fe^{3+}_{Blo}$	2 La^{3+} and 6 Sr^{2+}	0.04	0.13	0.09	6

[a] $N_{conf.}$ is the number of tested point-defect configurations.

view, the vacancy location in the O1 and O3 positions requires a substantially higher energy. The energetic difference (ΔE) between the two latter sites and O4 is as large as +0.52 and +0.75 eV, respectively.

A similar tendency was revealed for the hole generation in the oxygen-stoichiometric RP lattice. Namely, Fe^{4+} states exhibit a strong preference for the equatorial B1−O4 plane; the energetic difference (ΔE) between B1 and B2 layers is −0.44 eV (Table 1). This should correlate with a higher hole delocalization due to the presence of a pseudo-3D network formed by the $Fe_{B1}-O_{O2}-Fe_{B2}$ and $Fe_{B1}-O_{O4}-Fe_{B1}$ bonds. At the same time, Coulombic repulsion between Fe^{4+} and oxygen vacancies excludes their location in nearest-neighboring sites (ΔE = +1.16 eV, Table 2), unless the relatively stable ternary clusters $Fe^{4+}-V_O-Fe^{2+}$ are formed owing to trivalent iron disproportionation, $2Fe^{3+} \Leftrightarrow Fe^{4+} + Fe^{2+}$. The latter reaction should be taken into account for the analysis of high-temperature redox equilibria in ferrites[23−25] but can be neglected under oxidizing conditions when the electronic subsystem is dominated by holes generated due to oxygen intercalation. The same statement is true for Fe^{2+} states which could be, in fact, ignored in the range of conditions studied in this work, as their concentration at $\delta < 1$ is negligibly small. Nonetheless, the calculated energetic effects related to Fe^{2+} formation may be useful to analyze the redox behavior of dense $Sr_3La(Fe,Al)_3O_{10-\delta}$ membranes exposed to reducing atmospheres. In particular, the energetically unfavorable vacancy location in the O1 and O3 positions is predicted to promote $Fe^{2+}O_4$ tetrahedra formation in the central perovskite-like planes (Tables 1 and 2); this energetic affinity seems relevant for the appearance of brownmillerite-type slabs in the reduced RP ferrites.[1]

Doping with aluminum was found to induce further point-defect redistribution in $Sr_3La(Fe,Al)_3O_{10-\delta}$. The substitutional Al^{3+} ions can occupy both iron sites in the octahedral coordination typical for the oxidized lattice but display a substantial affinity for B1 positions when the coordination number decreases (Table 1). The latter effect, with $\Delta E = -1.1$ eV for 4-fold coordination, should also be promoted by the affinity of Al^{3+} to form pair and ternary clusters involving anion vacancies (Table 2). The results show that the preferential aluminum incorporation into the B1 sites[2] is primarily associated with oxygen deficiency arising at elevated temperatures necessary for solid-state synthesis and single crystal growth; on the subsequent reoxidation at lower temperatures, the Fe/Al site occupancy remains unchanged due to stagnated cation diffusion.

Whatever the thermodynamic stability of the dopant distribution, one important consequence relates to hole displacement from the nearest-neighboring B sites. When introducing a hole near $Al^{3+}O_4$ tetrahedron sharing one anion with the $Fe^{4+}O_6$ octahedron as illustrated in Figure 1b, the average energy increments are as high as 0.9−1.0 eV (Table 2). If a vacancy exists between Fe^{4+} and Al^{3+} (Figure 1c), the repulsion forces increase this energy up to 1.6 eV. Therefore, the accumulation of aluminum cations and oxygen vacancies in the equatorial perovskite layer is expected to displace Fe^{4+} from their preferential B1 positions. Moreover, if even the lattice is oxygen-stoichiometric, the presence of octahedrally coordinated Al^{3+} and Fe^{4+} in the adjacent sites causes modest but significant repulsion. The corresponding ΔE values, ~0.1 eV, are close to the typical level of small-polaron migration energies in perovskite-like ferrites.[23] The repulsive interactions originate, first of all, from local lattice distortions near Al^{3+}. As an example, the

(23) Goodenough, J. B.; Zhou, J.-S. In *Localized to Itinerant Electronic Transition in Perovskite Oxides*; Goodenough, J. B., Ed.; Springer-Verlag: Berlin, 2001; p 17.
(24) Mizusaki, J. *Solid State Ionics* **1992**, *52*, 79.
(25) Yoon, K. J. *J. Electrochem. Soc.* **2009**, *156*, B795.

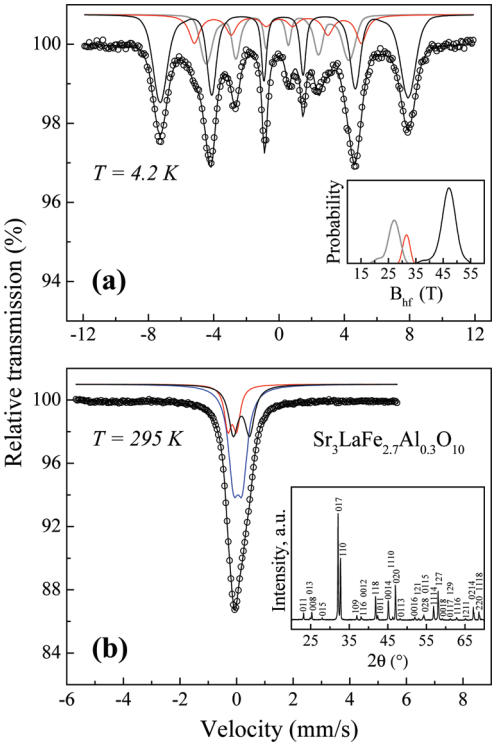

Figure 3. Mössbauer spectra of $Sr_3LaFe_{2.7}Al_{0.3}O_{10}$, collected at 4.2 K (a) and 295 K (b). The lines plotted over the experimental points are the sum of three hyperfine field distributions at 4.2 K and three quadrupole doublets at 295 K, shown shifted for clarity. Insets show the probability distributions of the magnetic hyperfine fields (a) and the XRD pattern indexed in the *I*4/*mmm* space group (b).

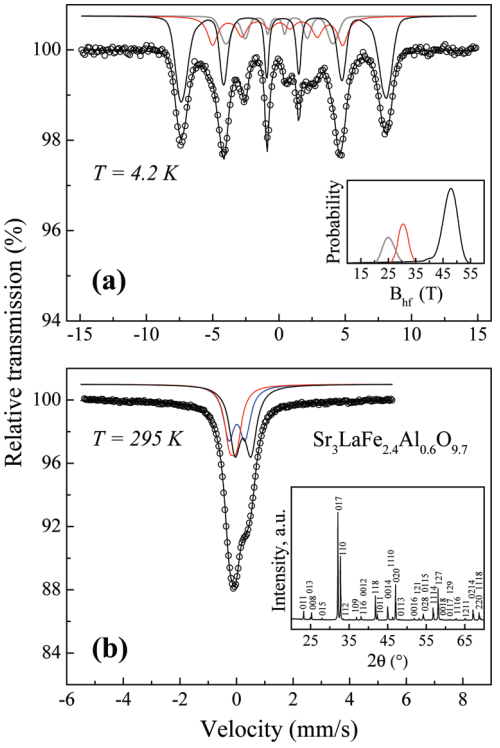

Figure 4. Mössbauer spectra of $Sr_3LaFe_{2.4}Al_{0.6}O_{9.72}$, collected at 4.2 K (a) and 295 K (b). The lines plotted over the experimental points are the sum of three hyperfine field distributions at 4.2 K and three quadrupole doublets at 295 K, shown shifted for clarity. Insets show the probability distributions of the magnetic hyperfine fields (a) and the XRD pattern indexed in the *I*4/*mmm* space group (b).

$Al^{3+}_{B1}-O^{2-}_{O2}$ and $O^{2-}_{O2}-Fe^{3+}_{B2}$ bonds become respectively 4% shorter and 3% longer compared to the analogous situation when the B1 site is occupied by Fe^{3+}. Such changes should influence the degree of hole localization. When the concentrations of Al^{3+} and/or oxygen vacancies become substantial, a complete reconfiguration of the electronic sublattice with massive hole displacement to the edge $B2O_6$ octahedra and a transition from itinerant to localized behavior of the p-type electronic charge carriers are therefore expected.

The conclusions regarding the hole redistribution and Al^{3+} effects were validated by the Mössbauer spectroscopy analysis of $Sr_3La(Fe,Al)_3O_{10-\delta}$. The spectra of $Sr_3LaFe_{2.7}Al_{0.3}O_{10}$ and $Sr_3LaFe_{2.4}Al_{0.6}O_{9.72}$ collected at 4.2 K are plotted in Figures 3a and 4a. As expected considering the broadness of the observed absorption peaks, when sextets of Lorentzian lines were used to fit the spectra, the estimated half-maximum line widths varied from 0.5 up to 1.1 mm/s for the inner and outer peaks of the sextets, respectively. Therefore, the final analyses were performed with a sum of distributions of magnetic hyperfine fields (B_{hf}). The line widths of each individual sextet in a distribution were kept equal to 0.26 mm/s, the experimental value of a single Lorentzian-line width in the calibration spectrum obtained for a metallic α-Fe foil. The 4.2 K spectra of $Sr_3LaFe_{2.7}Al_{0.3}O_{10}$ and $Sr_3LaFe_{2.4}Al_{0.6}O_{9.72}$ (Figures 3a and 4a) clearly show the presence of Fe^{3+} and Fe^{5+} formed due to the low-temperature disproportionation of tetravalent iron. Fitting of these spectra to the model[3] that only comprises Fe^{3+} and Fe^{5+} leads however to overestimated average oxidation states of iron cations; the resultant oxygen content calculated using the crystal electroneutrality condition appears in contradiction to the TGA data. As an example, the $[Fe^{3+}]/[Fe^{5+}]$ concentration ratio estimated by this model for $Sr_3LaFe_{2.7}Al_{0.3}O_{10}$ is 1.33, which corresponds to ~10.16 oxygen anions per formula unit. Such a deviation is much higher than the standard experimental uncertainties, 0.02 oxygen atoms per unit formula for TGA and 2% for the Mössbauer signal relative areas (*I*). Furthermore, a careful analysis of the 4.2 K spectra reveals the features described earlier for perovskite-type (A,Ln)(Fe,Al)O_3 (A = Sr, Ba; Ln = La, Pr, Nd).[19−21,26] As for these perovskites, the fitting quality is significantly improved when using the model with three distributions. The refined parameters of the additional component (Table 3) are characteristic of high-spin Fe^{4+};[19−21] the oxygen content calculated accounting for this state becomes very close to the TGA results, within the limits of experimental error.

The spectra collected at 295 K (Figures 3b and 4b) show only a single absorption peak with a shoulder on the high-velocity side. At room temperature the RP ferrites are paramagnetic, and all the signals consist of doublets; due to their overlapping, no resolved peaks are observed. The

(26) Kharton, V. V.; Kovalevsky, A. V.; Patrakeev, M. V.; Tsipis, E. V.; Viskup, A. P.; Kolotygin, V. A.; Yaremchenko, A. A.; Shaula, A. L.; Kiselev, E. A.; Waerenborgh, J. C. *Chem. Mater.* **2008**, *20*, 6457.

Table 3. Parameters[a] Estimated from the Mössbauer Spectra of $Sr_3La(Fe,Al)O_{10-\delta}$

composition and unit cell parameters	T (K)	Fe state	IS (mm/s)	QS,2ε (mm/s)	B_{hf} (T)	I (%)	δ
$Sr_3LaFe_{2.7}Al_{0.3}O_{10}$	4.2	3+	0.41	0.04	46.9	55	0.01
		4+ (localized)	0.08	−0.10	32.1	17	
a = 3.8621(1) Å		5+	0.01	0.02	26.7	28	
c = 28.086(9) Å	295	3+	0.29	0.54		28	
		4+ (localized)	−0.04	0.31		18	
		4+ (itinerant)	0.14	0.33		54	
$Sr_3LaFe_{2.7}Al_{0.3}O_9$	4.2	3+	0.42	−0.03	54.6	28	1.0
		3+	0.46	−0.44	51.2	20	
a = 3.8770(5) Å		3+	0.44	−0.64	54.0	52	
c = 28.238(9) Å	295	3+	0.33	0.03	42.3	29	
		3+	0.36	−0.39	38.9	21	
		3+	0.35	−0.50	42.1	50	
$Sr_3LaFe_{2.4}Al_{0.6}O_{9.72}$	4.2	3+	0.43	0.06	47.3	56	0.28
		4+ (localized)	0.09	−0.09	30.0	28	
a = 3.8607(4) Å		5+	0.03	0.25	25.2	16	
c = 28.174(4) Å	295	3+	0.34	0.56		41	
		4+ (localized)	−0.01	0.25		28	
		4+ (itinerant)	0.12	0.57		31	

[a] IS, B_{hf}, QS, 2ε, I, and T are the isomer shift relative to α-Fe at room temperature, magnetic hyperfine field, quadrupole splitting, quadrupole shift, relative area, and measurement temperature, respectively. Estimated standard deviations are ≤2% for I, < 0.2 T for B_{hf}, and < 0.02 mm/s for all other parameters.

conclusions concerning the presence of particular iron states and their ratio can therefore be based only on the 4.2 K spectra. It is, however, possible to show that the model consistent with that for the low-temperature data is applicable for the analysis of 295 K spectra, which were hence fitted to three quadrupole doublets (Table 3). The estimated line widths vary in the ranges 0.43−0.48 and 0.31−0.44 mm/s for $Sr_3LaFe_{2.4}Al_{0.6}O_{9.72}$ and $Sr_3LaFe_{2.7}Al_{0.3}O_{10}$, respectively. In the former compound, the peaks are broader due to an increased disorder arising from the higher dopant and oxygen-vacancy concentrations. As the temperature increases, the recoil-free fraction f for the iron species with weaker bonding might be expected to decrease faster, thus leading to underestimation of their amount at 295 K. However, for the majority of available literature data on perovskite-related oxides studied in the low-temperature range and at room temperature, this effect is usually found within the limits of experimental error associated with the estimation of relative areas.[17,18,20,21,26−28] Therefore, it seems reasonable that in the present case differences in f appear also not to affect significantly the I values up to 295 K (Table 3). The isomer shifts (IS) of itinerant Fe^{4+} disproportionating at 4.2 K are considerably larger compared to the Fe^{4+} states exhibiting no charge disproportionation, again confirming a higher electron localization in the latter case.[18] Notice also that no phase impurities were identified by XRD; fragments of the corresponding XRD patterns are presented in the insets of Figures 3b and 4b.

For oxidized $Sr_3LaFe_{2.7}Al_{0.3}O_{10}$, the calculated concentration ratio $[Fe^{4+}]/([Fe^{3+}]+[Al^{3+}])$ is very close to 2:1, the ideal B2:B1 ratio in the n = 3 RP structure. This proportion may indicate that the p-type electronic charge carriers are indeed displaced into the B2 layers, while B1 positions are predominantly occupied by Fe^{3+} and Al^{3+}. Assuming that delocalization may only occur for the Fe^{4+}_{B2} states located near Fe^{3+}_{B1} and cannot take place if Al^{3+}_{B1} is present in the hole nearest neighborhood, at room temperature the concentration of itinerant Fe^{4+} should then be twice as high as the Fe^{3+} amount. At 4.2 K when all itinerant Fe^{4+} states are disproportionated into Fe^{3+} and Fe^{5+}, the concentration of Fe^{5+} should appear equal to the room-temperature content of trivalent iron. Indeed, the experimental values (Table 3) are almost equal to these ideal relationships; the deviations are 4% or lower. Hence, the local distortions near aluminum cause localization of the Fe^{4+}_{B2} states adjacent to Al^{3+}_{B1}; only the iron cations forming $Fe_{B2}-O_{O2}-Fe_{B1}$ bonds enable hole delocalization and low-temperature disproportionation.

A very similar situation is observed for $Sr_3LaFe_{2.4}Al_{0.6}O_{9.72}$, where the aluminum content and oxygen deficiency are both higher than those in $Sr_3LaFe_{2.7}Al_{0.3}O_{10}$ and a part of Fe^{3+} cations are thus located in the B2 sites. If all Al^{3+} occupy B1 positions, the theoretical expectation for possible maximum content of Fe^{5+} formed due to the low-temperature disproportionation of itinerant Fe^{4+} would be approximately equal to the concentration of remaining B1 sites occupied by iron, that is, 0.40 per $Sr_3LaFe_{2.4}Al_{0.6}O_{9.72}$ formula unit. The experimental value calculated from the 4.2 K MS data (Table 3) is 0.38. One should also mention that, for the oxygen-deficient lattice where the formation of Al^{3+}_{B1} O_4 tetrahedra is energetically favorable, the energetic difference between two defect configurations shown in Figure 1b,c should lead to an additional limitation. Namely, each Al^{3+}_{B1} O_4 tetrahedron may have, at maximum, one nearest-neighboring Fe^{4+}_{B2} as the formation of $Fe^{4+}_{B2}-V_{O2}-Al^{3+}_{B1t}$ bonds is very unlikely (Table 2). The MS data show indeed that the concentration of localized Fe^{4+} in $Sr_3LaFe_{2.4}Al_{0.6}O_{9.72}$ is close to Al^{3+} concentration. Therefore, the results on oxidized $Sr_3LaFe_{3-x}Al_xO_{10-\delta}$ (x = 0.3−0.6,

(27) Dann, S. E.; Currie, D. B.; Weller, M. T.; Thomas, M. F.; Al-Rawwas, A. D. *J. Solid State Chem.* **1994**, *109*, 134.
(28) Gibb, T. C. *J. Solid State Chem.* **1988**, *74*, 176.

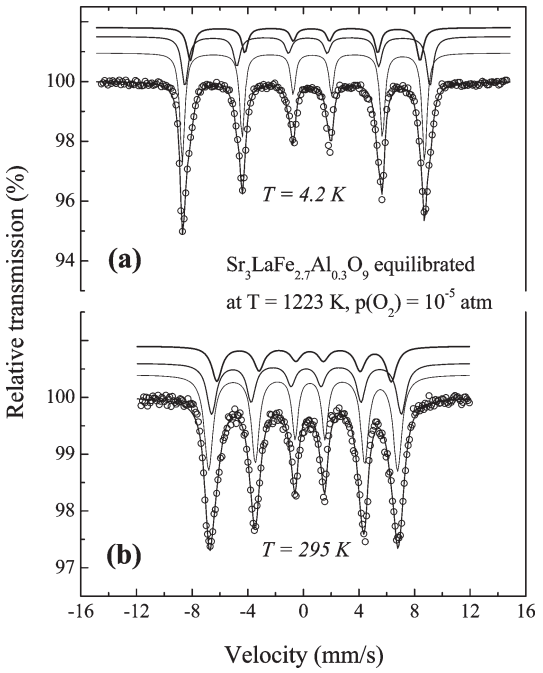

Figure 5. Mössbauer spectra of $Sr_3LaFe_{2.7}Al_{0.3}O_9$ at 4.2 K (a) and 295 K (b). The lines plotted over the experimental points are the sum of three magnetic sextets, shown shifted for clarity.

$\delta = 0-0.28$) confirm major conclusions drawn on the basis of computer simulation studies, which predicted the hole displacement in the apical iron−oxygen polyhedra by Al^{3+} occupying B1 positions and significant effects of aluminum cations on the nearest-neighboring iron sites, including strong repulsion between Fe^{4+} and Al^{3+}_{B1} O_4 tetrahedra. In fact, the deviations from the ideal defect-concentration ratios predicted by atomistic simulations are as low as 4−5%, comparable to the cumulative errors.

While most B2 sites adjacent to Fe^{3+}_{B1} in the oxidized $Sr_3LaFe_{2.7}Al_{0.3}O_{10}$ and $Sr_3LaFe_{2.4}Al_{0.6}O_{9.72}$ lattices are occupied by Fe^{4+}, another defect distribution can be expected for $Sr_3LaFe_{2.7}Al_{0.3}O_9$ where the content of the tetravalent iron, if any, is lower than the MS detection limits. Analysis of the $Sr_3LaFe_{2.7}Al_{0.3}O_9$ spectra (Figure 5) made it possible to identify at least three contributions, all related to Fe^{3+} cations in different local environments; their estimated parameters are summarized in Table 3. No further improvement of the fitting quality was achieved when introducing an extra signal. Two of the components show significant quadrupole perturbations with quadrupole shifts (ε) much higher than for the samples annealed in air. The large negative ε values are typical for octahedral Fe^{3+} in the brownmillerite-type oxides (e.g., refs 29 and 30 and references therein) and might be indicative of similar ordering processes in highly deficient $Sr_3La(Fe,Al)_3O_9$, as recently reported for $Sr_3NdFe_3O_9$.[1] Indeed, these two signals yield the total concentration of Fe^{3+} close to the fraction of B2 positions, namely, 1.94 cations per formula unit. The sextet having higher IS and lower B_{hf} seems to originate from Fe^{3+}_{B2} located near Al^{3+}_{B1}; the corresponding fraction of trivalent iron (0.54 per formula unit) is quite close to double Al^{3+} concentration, whereas the presence of Al^{3+} nearest neighbors breaking the $Fe^{3+}-O-Fe^{3+}$ magnetic exchange interactions should decrease B_{hf}. Notice that the atomistic computer simulations demonstrated a strong energetic affinity of aluminum cations to form Al^{3+}_{B1} O_4 tetrahedra (Table 2). The average energetic difference between Al^{3+}_{B1} O_4 and similar Fe^{3+}_{B1} O_4 tetrahedra is as high as 1.6 eV. This factor, in agreement with experimental data on $Ca_2(Fe,Al)_2O_5$ brownmillerite,[29] is responsible for the dominant six- and fivefold coordination of the remaining Fe^{3+}_{B1} as indicated by the relevant IS and B_{hf} values (Table 3).

Finally, the results show that the alterations in defect chemistry of $Sr_3La(Fe,Al)_3O_{10-\delta}$ induced by Al doping and/or oxygen deintercalation should have a strong influence on the transport properties and stability. First of all, the preferable vacancy location in the central $B1O_6$ layers and hole displacement out from these layers increase two-dimensional character of the ionic and electronic conduction, which is characteristic of $n = 1$ RP phases and is unusual for disordered perovskite systems. The changes in the electronic sublattice and, in particular, progressive hole localization are expected to shift the electron−hole equilibrium toward n-type charge carriers. For other perovskite-related ferrites,[6] such phenomena are accompanied with decreasing thermodynamic stability on reduction. The same factor can explain the accentuated affinity of the $n = 3$ RP ferrites for hydration and carbonation, reported for the Nd-containing analogue[1] and observed in this work.

4. Conclusions

The atomistic computer simulations and ^{57}Fe transmission Mössbauer spectroscopy analysis of $Sr_3LaFe_{3-x}Al_xO_{10-\delta}$ ($x = 0.3-0.6$) provide a clear evidence that the introduction of point defects, such as Al^{3+} and oxygen vacancies, into the central perovskite layers of $n = 3$ RP ferrite structure may lead to a complete reconfiguration of the electronic sublattice. Namely, the local lattice distortions near Al^{3+} and repulsion between the positively charged vacancies and holes induce massive hole displacement out of the energetically favorable equatorial B1 planes to the edge $B2O_6$ octahedra, accompanied with progressive localization. Increasing oxygen deficiency results in the appearance of relatively stable aluminum−oxygen tetrahedra in the central perovskite-type layers, which are among the most favorable defect configurations revealed by atomistic modeling and have strong effects on the nearest-neighboring iron sites. These phenomena are expected to increase two-dimensional character of the ionic and electronic conduction in the $n = 3$ RP ferrites and to decrease their stability.

Acknowledgment. This work was partially supported by FCT, Portugal (Projects PTDC/CTM/64357/2006 and SFRH/BPD/28629/2006).

(29) Waerenborgh, J. C.; Rojas, D. P.; Vyshatko, N. P.; Shaula, A. L.; Kharton, V. V.; Marozau, I. P.; Naumovich, E. N. *Mater. Lett.* **2003**, *57*, 4388.
(30) Battle, P. D.; Gibb, T. C.; Nixon, S. *J. Solid State Chem.* **1988**, *73*, 330.